Extraction and Characterization of Modified Algae Derivative Cellulose and its Mixtures for Dye Removal

Md. Rezaur Rahman,[a,*] Anthonette Anak James,[a] Al-Khalid bin Othman,[a] Muhammad Khusairy Bin Bakri,[a] Jamal Uddin,[g] Ain Zaienah Sueraya,[a] Mohammed Mahbubul Matin,[b] Sulaiman Y. Alfaifi,[c] O. Madkhali,[d] Mahmood D. Aljabri,[e] and Mohammed M. Rahman [f]

A new bio-sorbent derived from green algae biomass, *Arthrospira platensis* (Spirulina), was found to be economically practical for water decontamination. This biosorbent comprised of microalgae cellulose, poly(lactic acid) (PLA), Dabai activated carbon (AC), and montmorillonite (MMT), each plays a distinctive role in removing methylene blue (MB) dye. The presence of hydroxyl and carbonyl functional groups in algae cellulose, confirmed by the FTIR analysis, offered binding sites for dye removal. Scanning electron microscopy demonstrated the morphological structure of the biosorbent, highlighting the combined effect of microalgae cellulose, PLA, Dabai AC, and MMT mixtures. The inclusion of Dabai AC and MMT improved micropores and mesopores, enhancing adsorption reactions. The Brunauer-Emmett-Teller (BET) analysis confirmed that the sample containing microalgae cellulose, Dabai AC, and MMT clay in PLA had a specific surface area of 0.784 m^2/g, three times higher than the PLA + cellulose sample. Additionally, adding 1% MMT to the sample improved the particle dispersion on the surface of the hydrophobic PLA, thereby improving its thermal properties. Remarkably, the biosorbent effectively eliminated 86.8% of MB dye from an initial concentration of 50 mg/L after 60 min of Vis-light irradiation using Ultraviolet-visible spectroscopy.

DOI: 10.15376/biores.18.3.5967-5992

Keywords: Algae; Cellulose; Mixtures; Synthesis; Clay

*Contact information: a: Faculty of Engineering, Universiti Malaysia Sarawak, Jalan Datuk Mohammad Musa, Kota Samarahan, Sarawak, Malaysia; b: Bioorganic and Medicinal Chemistry Laboratory, Department of Chemistry, Faculty of Science, University of Chittagong, Chittagong, Bangladesh; c: Department of Chemistry, King Abdulaziz University, Jeddah 21589, Saudi Arabia; d: Department of Physics, College of Science, Jazan University, P.O. Box 114, Jazan 45142, Kingdom of Saudi Arabia; e: Department of Chemistry, University College in Al-Jamoum, Umm Al-Qura University, Makkah 21955, Saudi Arabia; f: Center of Excellence for Advanced Materials Research (CEAMR), King Abdulaziz University, Jeddah 21589, Saudi Arabia; g: Department of Natural Science, Coppin State University, Science and Technology Center, Baltimore, Maryland, 21216, U.S.A; *Corresponding author: rmrezaur@unimas.my*

INTRODUCTION

Approximately 700,000 tons of various colorants are produced annually, with 100,000 commercially available dyes used in industrial applications (Samsami *et al.* 2020). These dyes are frequently discarded into water bodies without further treatment. The textile industry generates 54% of dye effluent from using 75% of global dye for coloration and printing on fabrics, followed by the dyeing industry, which accounts for 21% (Slama *et al.* 2021). The failure of the dye mixture to adhere entirely to the fabric is the primary cause

of the high amount of dye effluent generation. Methylene blue (MB) dye is one of the most dangerous dye effluents released by the textile and tanning industries (Moghazy *et al.* 2020). The accumulation of dyes poses a significant threat to the environment as it reduces light penetration, preventing photosynthesis and lowering oxygen levels in the water. As a result, viruses and bacteria multiply, making the water unsafe to consume and use.

The environmental legislature has added a new law regarding the discharge of toxic colored effluent into the water bodies, which requires dye-utilizing industries to adhere to The International Dye Industry Wastewater Discharge Quality Standards. There are a few ways to remove dyes from water which include oxidation (Nidheesh *et al.* 2018; Alshahrani *et al.* 2022), adsorption (Harja *et al.* 2022; Sultana *et al.* 2022), flocculation-precipitation (Berber-Villamar *et al.* 2018), and membrane separation (Moradihamedani 2021). According to Royanudin *et al*. (2021), adsorption is one of the most widely used methods due to its simplicity, low cost, and high success rate. However, using bio-sorbent for adsorption has emerged as an appealing approach among researchers to treat domestic and industrial wastewater due to the need for more abundant, environmentally acceptable, cost-effective, and biodegradable materials (Moghazy and Abdo 2018; Aka *et al.* 2019; Qi *et al.* 2021; Biswas and Pal 2021). The unique characteristics of each bio-sorbent, including their adsorbing surface nature, pore structure, and porosity, have contributed to their diverse roles in the removal of dyes from industrial effluent. *Arthrospira platensis* (Spirulina), a promising natural inexhaustible source of raw materials, is suitable for developing algae-based biosorbents. The *Arthrospira platensis* (Spirulina) algae biomass is commonly used for heavy metal removal. However, there is limited information on its use for dye removal from wastewater. Algal biomass contains a variety of functional groups due to the presence of alginate gel in their cell walls, which may promote excellent binding sites (Moghazy *et al.* 2020). To date, no research has been reported on developing Spirulina algae biomass mixtures with the addition of activated carbon (AC), clay, and polymer to develop bio-sorbent.

This study aimed to synthesize cellulose from *Spirulina platensis* algae to develop environmentally friendly biosorbent mixtures with varying percentages of *Dabai* AC, montmorillonite (MMT) clay, and polylactic acid (PLA). Polylactic acid, MMT, and *Dabai* AC were chosen for their bio-derived properties. Dabai is a native fruit exclusively found in Borneo Island, and its nutshell was later on converted into an activated biocarbon. MMT, on the other hand, was used as a clay mineral, which contributes to the increased surface area and porous structure of the sample. In this work, the properties of the developed bio-sorbents were investigated *via* several characterization tests such as Fourier transform infrared spectroscopy (FTIR), scanning electron microscopy (SEM) with energy dispersive X-Ray analysis (EDX), Brunauer-Emmet-Teller (BET) analysis, and thermogravimetric analysis (TGA). To validate the ability of the developed bio-sorbent in treating dye effluent, a comparison study with commercial adsorbents was conducted.

EXPERIMENTAL

Materials

Dried green algae biomass provided by the Sarawak Biodiversity Center (SBC) was used as the main material for cellulose synthesis. Sodium hydroxide (NaOH) pellet (CAS Number: 1310-73-2), sodium chlorite ($NaClO_2$) (CAS Number: 80 7758-19-2), glacial acetic acid (CAS Number: 64-19-7), montmorillonite (MMT) (CAS Number: 1318-93-0),

polylactic acid (PLA) (CAS Number: 26100-51-6) and methylene blue (MB) dye (CAS Number: 61-73-4) were purchased from Merck. Dabai-activated carbon (AC) was provided by Universiti Malaysia Sarawak (UNIMAS).

Methods

Preparation of algae biomass, alkali, and bleach solution

The algal biomass was weighed and ground until forming a powder. The ground algae were then placed in a petri dish for further use. An amount of 0.4 g NaOH pellets were poured into a beaker filled with 250 mL distilled water and stirred until fully dissolved. The solution was transferred into a 1000 mL volumetric flask. The beaker was rinsed repeatedly with distilled water and poured into the volumetric flask until the liquid level was about 2 cm below the graduated mark. Next, distilled water was added using a dropper to the flask until the meniscus showed the same level as the graduated line. The volumetric flask was closed with a stopper and shaken. The flask was labeled as '0.01 M NaOH'.

A bleach solution was prepared with an equal volume of acetate buffer and aqueous sodium chlorite. Approximately 40.5 g of NaOH (MW: 39.997 $gmol^{-1}$) and 112.5 mL of glacial acetic acid were diluted to 1000 mL of distilled water and stirred until the mixture dissolved to produce acetate buffer with a pH of 4.74. The acetate buffer was kept in a 2000 mL screw cap bottle and labeled as 'acetate buffer.' Next, roughly 102 mL of 0.25 M NaClO2 was dissolved in 1398 mL distilled water to produce a 0.017 M NaClO2 solution. The $NaClO_2$ solution was then kept in a 2000 mL screw cap bottle labeled '0.017 M NaClO2'. Finally, 500 mL of each acetate buffer and NaClO2 were poured into a beaker for bleaching treatment.

Separation of cellulose from algae

The experiment was conducted with a ratio of 1:20 of algae biomass to the solution during the treatment. First, 50 g of ground algae was weighed and placed into a beaker with a weighing scale. Then, 1000 mL of distilled water was heated to 60 °C using a hotplate stirrer. The raw algae were then poured into the heated distilled water and stirred continuously for 1 h. After 1 h, the mixture was left to cool at room temperature until a separated layer was formed. The top layer was poured as waste, leaving the bottom layer filled with wet algae. The cellulose extraction was conducted as described by Sebeia *et al*. (2019). A volume of 1000 mL of 0.01 M NaOH was heated to 80 °C to prepare for alkali treatment. Wet algae were then poured into the heated NaOH and stirred continuously for 1 h. Following the treatment, the mixture was allowed to cool to room temperature, and distilled water was gradually added until a supernatant layer formed in the solution.

The top layer was poured out as waste, leaving the bottom layer of alkali-treated algae. The bleach solution was made with an equal amount of acetate buffer and aqueous $NaClO_2$ and then heated to 80 °C. The alkali-treated algae were poured into the bleach solution and treated three times again for 40 min under continuous stirring until pure white-colored cellulose was obtained. The mixture was then left to cool before pouring into the centrifuge tube and centrifuged for 15 min at 15000 RPM using a centrifuge machine. After centrifugation, the top layer was poured out, leaving the bleached algae cellulose at the bottom. Next, distilled water was added to the bleached algae-containing tube, mixed, and put for centrifuged again to obtain pH 7. The cellulose was poured into a petri dish once pH 7 was obtained and placed in a drying oven at 60 °C for 6 h. The dried cellulose was left to cool to room temperature, ground with a mortar and pestle, and kept for further use.

Preparation of sample

The mixtures were prepared by blending the materials in accordance with the compositions shown in Tables 1, 2, 3, and 4. The purpose of blending was to ensure the materials were thoroughly mixed and resulted in a homogeneous mixture. The mixture ratios were estimated using the maximum and minimum values found in the literature.

Table 1. PLA

Sample	PLA (wt%)	Total (wt%)
1	100	100

Table 2. PLA + Cellulose

Sample	PLA (wt%)	Cellulose (wt%)	Total (wt%)
1	98.0	2.0	100
2	99.0	1.0	100
3	99.5	0.5	100

Table 3. PLA + Cellulose + AC

Sample	PLA (wt%)	Cellulose (wt%)	AC (wt%)	Total (wt%)
1	96.0	2.0	2.0	100
2	97.0	2.0	1.0	100
3	97.5	2.0	0.5	100

Table 4. PLA + Cellulose + AC + MMT

Sample	PLA (wt%)	Cellulose (wt%)	AC (wt%)	MMT (wt%)	Total (wt%)
1	95.0	2.0	2.0	1.0	100
2	96.0	2.0	1.0	1.0	100
3	97.0	1.0	1.0	1.0	100

Dye adsorption test

First, 0.1 g of MB dye powder was dissolved in distilled water in a 250 mL beaker, and the solution was transferred into a 500 mL volumetric flask. The beaker was then rinsed repeatedly with distilled water and poured into the volumetric flask until the liquid level was 2 cm below the graduated mark. The volumetric flask was closed with a stopper and shaken. The flask was labeled as '200 ppm MB'. Then, 250 mL of 200 ppm MB was taken from the flask and placed into a beaker. The solution in the beaker was poured into a 1000 mL volumetric flask.

Similarly, the beaker was then rinsed repeatedly with distilled water and poured into the volumetric flask until the liquid level was about 2 cm below the graduated mark. Distilled water was added to the flask until the meniscus showed the same level as the graduated line using a dropper. Again, the volumetric flask was closed with a stopper and shaken. Finally, the flask was labeled as '50 ppm MB' and kept aside for the application of dye adsorption.

Dye adsorption was done using the samples of microalgae cellulose, 100% PLA, PLA + 2% cellulose, PLA + 2% cellulose + 2% AC, and PLA + 2% cellulose + 2% AC + 1% MMT. Due to the fast adsorption of the samples, the time taken for the adsorption of MB dye was set to 60 min with 10 min interval for sample taking. Mixing the adsorbent and adsorbate was kept constant at 150 RPM. 5 beakers were prepared, and 1000 mL of 50 ppm MB was poured into each beaker. 1.0 g of each sample was weighed. Then, the

adsorbents were poured into the beaker and stirred continuously for 60 min using a hotplate stirrer and a magnetic stirrer. At every 10 min interval, 10 to 15 mL of samples were extracted using a syringe and filtered with filter paper into a centrifuge tube. The samples were then labeled accordingly and measured using UV-vis.

Characterizations and Tests

FTIR analysis of the neat PLA, algae cellulose, and developed mixtures

An FTIR spectrophotometer (Shimadzu, Kyoto, Japan) was used in a spectral range between 4000 to 400 cm^{-1} to examine the functional groups of the neat PLA, algae cellulose, and the mixture samples. Approximately 0.1 to 1.0% of the samples were mixed with 200 mg of dry potassium bromide (KBr) on a small pestle to create a small pellet. The analysis was started once the FTIR software was programmed following ASTM E1252-98 (2021) and ASTM E168-16 (2016) standards.

SEM-EDX analysis of the neat PLA, algae cellulose, and developed mixtures

The neat PLA, algae cellulose surface morphology, and the developed mixtures were observed using a Hitachi analytical tabletop SEM (benchtop) (TM-3030, Hitachi High Technologies, Mannheim, Germany) under an accelerating voltage of 15.0 kV. The characterization procedure was based on the ASTM E2015-04 (2014) standard. The elemental compositions of the samples were analyzed using EDX. Dried powdered samples were pasted on the SEM disc and placed in the chamber. The chamber was then let to EVAC before obtaining the results from the SEM and EDX software.

TGA analysis of the mixtures

The thermal stability of the algae cellulose biosorbent and its mixtures were analyzed using the TG machine. The dried samples were then heated from 25 to 700 °C at 10 °C/min, kept in a zip and lock bag, and handed to the laboratory assistants for analysis. The test was done according to ASTM E1131-20 (2020) standard.

BET analysis of the mixtures

The surface area of the mixtures labeled PLA + 2% cellulose, PLA + 2% cellulose + 2% AC, and PLA + 2% cellulose + 2% AC + 1% MMT were analyzed using the BET surface analyzer. The condition of the BET analysis was set at the degassing condition of 10 °C/min at 25 to 1000 °C for 6 h. The sample was dried by placing it in an oven at 60 °C. Upon drying, the sample was kept in a zip and lock bag and handed to the laboratory assistants for analysis. The test was based on the ASTM D6556-14 (2014) standard.

UV-vis analysis

The adsorption capacity of the cellulose, PLA, PLA + 2% cellulose, PLA + 2% cellulose + 2% AC, and PLA + 2% cellulose + 2% AC + 1% MMT were measured using a UV-vis spectrophotometer with wavelength ranging between 500 and 700 nm. Then 3 to 4 mL of samples were dropped into the UV-vis cuvette and placed into the UV-vis spectrophotometer to obtain the analysis results. The test was done according to ASTM E169-16 (2016). The biosorption capacity of the samples was calculated using the equation adopted from Paska *et al.* (2014) for evaluating the adsorption capacity (Eq. 1) and the methylene blue dye removal percentage (Eq. 2).

$$q_t = \frac{(C_o - C_t)V}{W} \quad (1)$$

$$\text{Dye removal (\%)} = \frac{(C_o - C_e)}{C_o} = 100 \quad (2)$$

In these equations, q_t is the dye absorbed per unit of biosorbent (mg/g); C_o is the concentration of dye at initial state(mg/L); C_t is the concentration of dye at different periods of time (mg/L); W is the weight of biosorbent (g); V is the volume of solution (L); and C_e is the concentration of dye at equilibrium (mg/L)

RESULTS AND DISCUSSION

FTIR analysis

The appearance of new peaks and the differences in intensities were considered based on the FTIR results in Fig. 1. The absorption bands of cellulose, Dabai AC, and MMT in Figs. 1 (a), (c) and (d) were observed between the regions of 400 to 4000 cm^{-1}. In contrast, the absorption bands of PLA, PLA/C, PLA/C/AC, and PLA/C/AC/MMT in Figs. 1 (b), (e), (f), and (g) were identified in the wavenumber range of 400 to 2000 cm^{-1}. Based on the peaks in Fig. 1**,** the peak at 3277 cm^{-1} revealed an O-H stretching vibration of the hydroxyl group in cellulose. The appearance of the O-H hydroxyl group was similar to the result of algae cellulose reported by Sebeia *et al*. (2019) through the detection of an absorbance band at 3292 cm^{-1}. The peaks between 1630 to 900 cm^{-1} were the typical absorbance bands observed in cellulose (Hospodarova *et al.* 2018). A sharp peak observed at 1638 cm^{-1} was attributed to the O-H bending variation of water molecules. This peak indicated the presence of water absorption within the void spaces of cellulose after the removal of lignin and hemicellulose (Liew *et al.* 2015). This finding further supported the hygroscopic behavior of cellulose in absorbing and retaining moisture from its surroundings. Other studies conducted by Samia *et al*. (2016) and Aragaw and Bogale (2021) discussed that the peak within the range of 1510 to 1650 cm^{-1} was responsible for C=O stretching variations. This possibly indicated the presence of the carbonyl group found in various compounds containing carboxylic acids, ketones, amides, aldehydes, and esters. Based on Mallamace *et al.* (2014), the band of amide I, which represented the stretching vibration of the C=O commonly observed within the range of 1600 to 1700 cm^{-1}, whereas the band of amide II, which showed the combination of N-H bending and C-N stretching vibration, is commonly observed in the range of 1500 to 1570 cm^{-1}. In Fig. 1(a), the appearance of the peak at 1650 cm^{-1} could also be due to the presence of amide I, whereas the peak at 1526 cm^{-1} was due to amide II. The presence of several polysaccharide components and proteins allowed the formation of acid-binding sites on the surface of microalgae which results in biosorbents with a high affinity toward dye (Singh *et al*. 2018; Siddiqui *et al.* 2019). Both Figs. 1 (a) and (c) showed the appearance of the C=O stretching variation. This makes it an appealing material for dye removal. In addition, the presence of a strong band at 1749 cm^{-1} in Fig. 1 (b), referred to as the C=O stretch, resulted in a more pronounced occurrence of peaks at 1749, 1748, and 1748 cm^{-1} in Figs. 1 (e), (f), and (g) of the mixture samples. Besides, the presence of the inorganic compounds in the lignocellulosic samples of cellulose and AC also caused the appearance of peaks corresponding to the C=O carbonyl stretch that indicate the presence of carboxylic acid functional groups. However, comparative studies revealed that the intensities of the peaks in the mixture samples were lower than that of pure PLA in Fig. 1 (b).

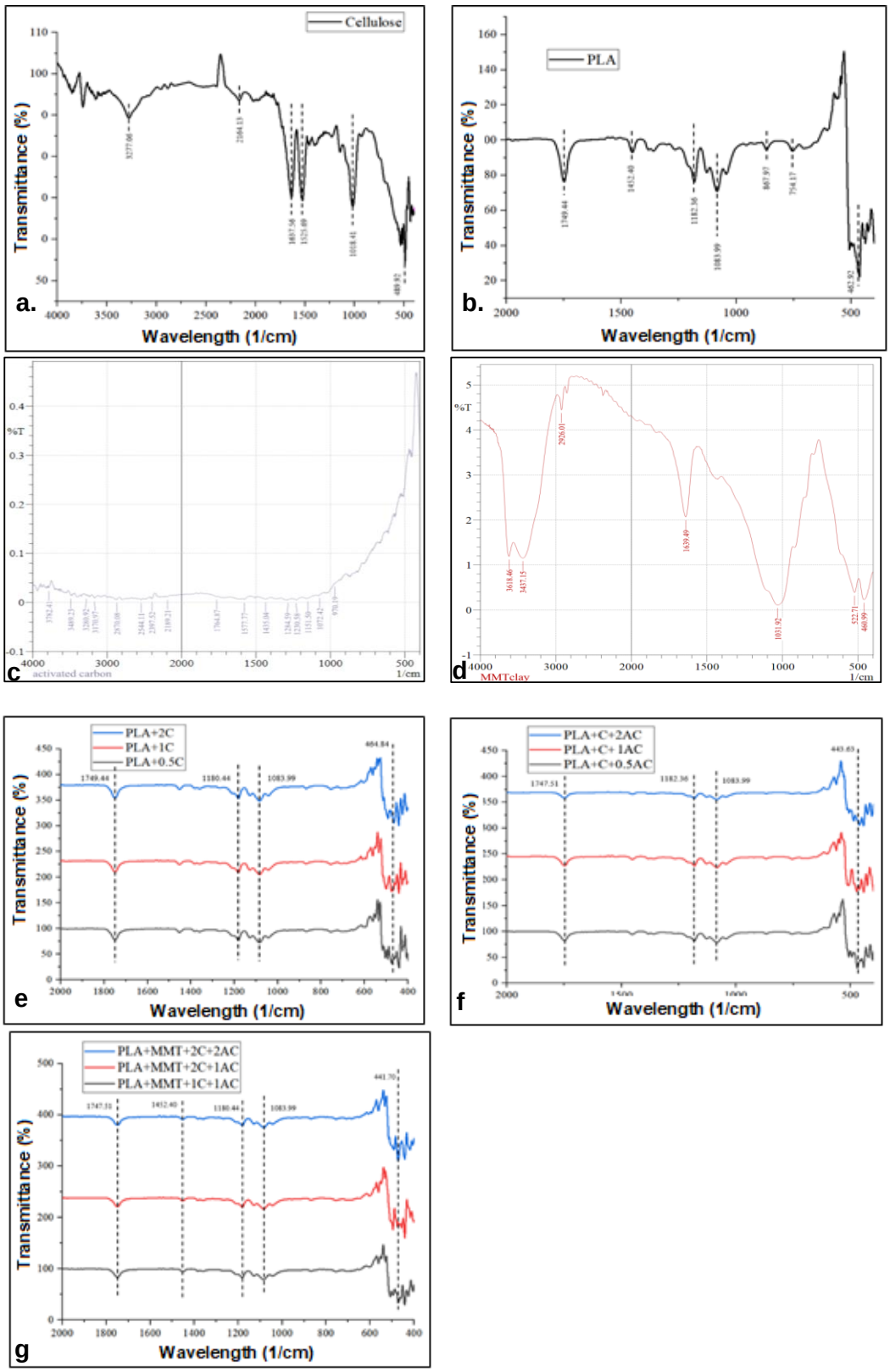

Fig. 1. FTIR spectra (a) cellulose; (b) pure PLA; (c) Dabai AC; (d) MMT; (e) PLA + cellulose; (f) PLA + cellulose + AC; (g) PLA + cellulose + AC + MMT

Besides, the peak at 1452 cm^{-1} shown by the PLA spectrum corresponds to the CH_3 asymmetric bending vibration, which also appeared at 1452 cm^{-1} (Chieng *et al.* 2013). Meanwhile, the peak at 1182 cm^{-1} demonstrates the characteristic of C-O-C stretching in PLA, which has also been observed in the spectra of PLA/C, PLA/C/AC, and PLA/C/AC/MMT mixtures. The C-O stretching frequency showed the characteristic of an ester group at wavenumber 1084 cm^{-1} in Figs. 1 (b), (e), (f), and (g), similar to the findings reported by Khui *et al.* (2021), James *et al.* 2022 and Choksi and Desai (2017). However, the peak intensities were slightly lower in Figs. 1 (e), (f), and (g) due to the addition of cellulose, AC, and MMT in the respective mixtures, which could influence the thermal properties displayed by the TGA results, as indicated by Deng *et al.* (2020).

Meanwhile, in Fig. 1 (d), the appearance of peaks at 1032 cm^{-1} and 529 cm^{-1} represented the Si-O stretching and bending vibrations. This observation aligned with the findings of Patel *et al.* (2006), who assigned the peak at 1035 cm^{-1} to Si-O stretching (in-plane), whereas the peak within the range of 1100 to 1000 cm^{-1} was assigned to the Si-O stretch (out-of-plane) for MMT. The appearance of the aforementioned peaks as well as the peak at 1084 cm^{-1} in Fig. 1 (g) indicated that the MMT had a good adhesion interaction with the composite (James *et al*. 2023). The FTIR results in Figs. 1 (f) and (g) showed a negligible difference in peak intensity. This provided evidence that the inclusion of 1% MMT clay had little effect on the FTIR results. Upon the addition of MMT to the mixtures, the intensity of the C-O-C asymmetric stretching peak at 1182 cm^{-1} in Fig. 1 (f) showed a slight reduction to 1180 cm^{-1}, as displayed in Fig. 1 (e), similar to the observation of Arjmandi *et al*. (2016). According to the authors, the reduction was initiated by the formation of hydrogen bonds between the MMT and PLA, which led to a good compatibility outcome. Hong *et al.* (2021) also indicated that the absorbance band of 1180 cm^{-1} was attributed to the glycosidic bonds which hold the cellulose units.

Two peaks at the wavenumber regions 868 and 754 cm^{-1} were attributed to the amorphous and crystalline phase of C-C stretching vibrations. These peaks were only visible in Fig.1 (b) of the pure PLA, since there were no obvious peaks in the mixture samples. The finding was similar to Rocca-Smith *et al.* (2017), who noticed peaks at 863 and 758 cm^{-1} in the FTIR result of a PLA film. The peaks of PLA/C in Fig. 1 (e) were more pronounced than the spectra of PLA/C/AC and PLA/C/AC/MMT mixtures in Figs. 1 (f) and (g). This indicates that the addition of AC and MMT to PLA/C does not affect the FTIR patterns of the mixtures, only their intensities due to the absence of a new functional group.

SEM/EDX analysis

The SEM results shown in Figs. 2, 3, 4, 5, and 6 are the morphological images of cellulose, pure PLA, PLA/C, PLA/C/AC, and PLA/C/AC/MMT at 800x magnification. Based on the observation, the cellulose structure derived from algae, as depicted in Fig. 2, exhibits a coarse surface due to several chemical treatments during the extraction. Similar to the morphological characteristic of *Aegagropila Linnaei* macroalgae (Sebeia *et al.* 2019), cellulose's rough surface can increase the likelihood of trapping numerous dye molecules. The presence of mesopores and micropores on the structures of microalgae increases the surface area of the material. This expanded surface area offers more available binding sites for the adsorption of dye molecules. In addition, the dissolution of algae fiber in an aqueous alkali solution caused a splitting effect and the formation of both intra- and intermolecular H-bonds, which changed the cellulose structure. Kannam *et al*. (2017) reported that the degradation of microfibrils resulted in numerous small particles

combining to form large microfibrils due to Van der Waals interaction and the effect of the hydrogen bond.

Figure 3 illustrates the morphological image of a pure PLA sample. PLA displays a smooth structural image compared to the samples of PLA/C, PLA/C/AC, and PLA/C/AC/MMT presented in Figs. 4, 5, and 6. A similar surface condition to Fig. 3 was noticed in Fig. 4 (a), although it contained 0.5% cellulose. As the percentage of cellulose increased, the sample structure exhibited small shallow cracks, causing slightly ductile behavior (Khui *et al.* 2021). More voids and deep crevasses (red circles) were created as AC and MMT were introduced to the sample, as observed in Figs. 5 and 6. This problem correlated with the one raised by Ramesh *et al*. (2019), who highlighted the importance of considering the concentration of MMT in a sample as it could affect its mechanical properties, causing the formation of micro-voids, accumulation, and fiber bending. However, there were no obvious agglomeration issues in any of the samples except for samples Figs. 5 (b) and (c), although there were poor dispersion and lack of interfacial interaction between the cellulosic particles and the PLA matrix due to the hydrophilic nature of cellulose (Sousa *et al.* 2019).

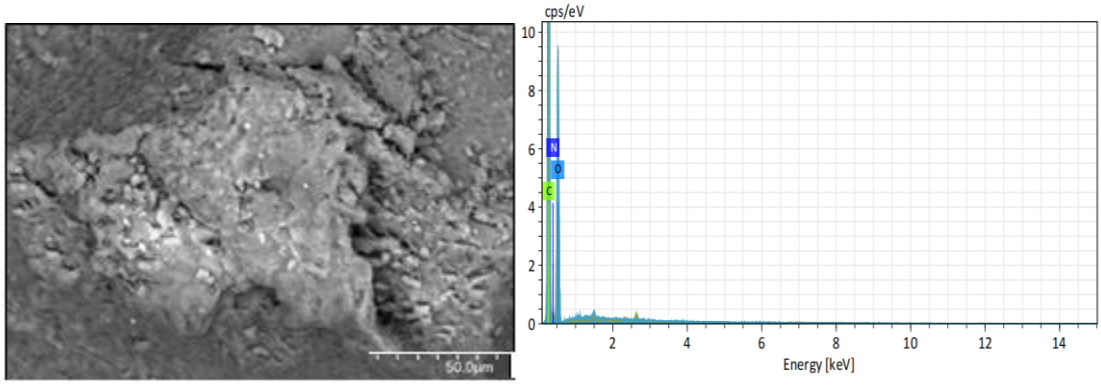

Fig. 2. SEM with EDX spectrum of cellulose at 800x magnification

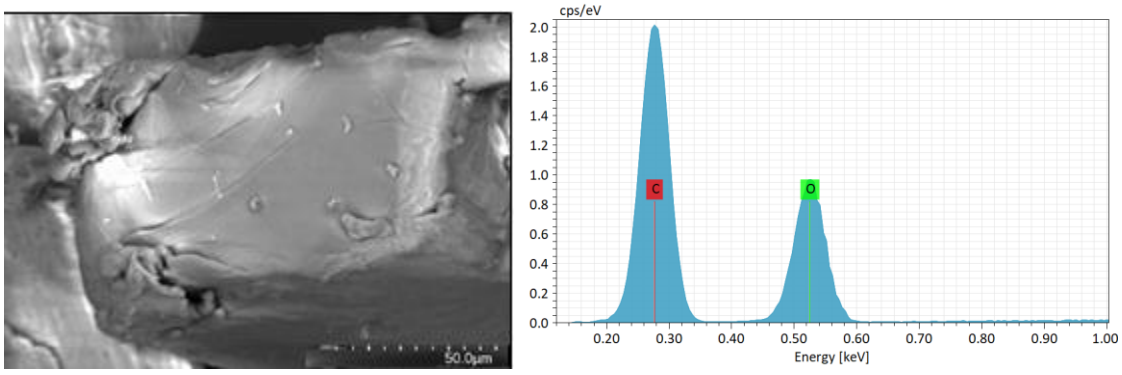

Fig. 3. SEM with EDX spectrum of pure PLA at 800x magnification

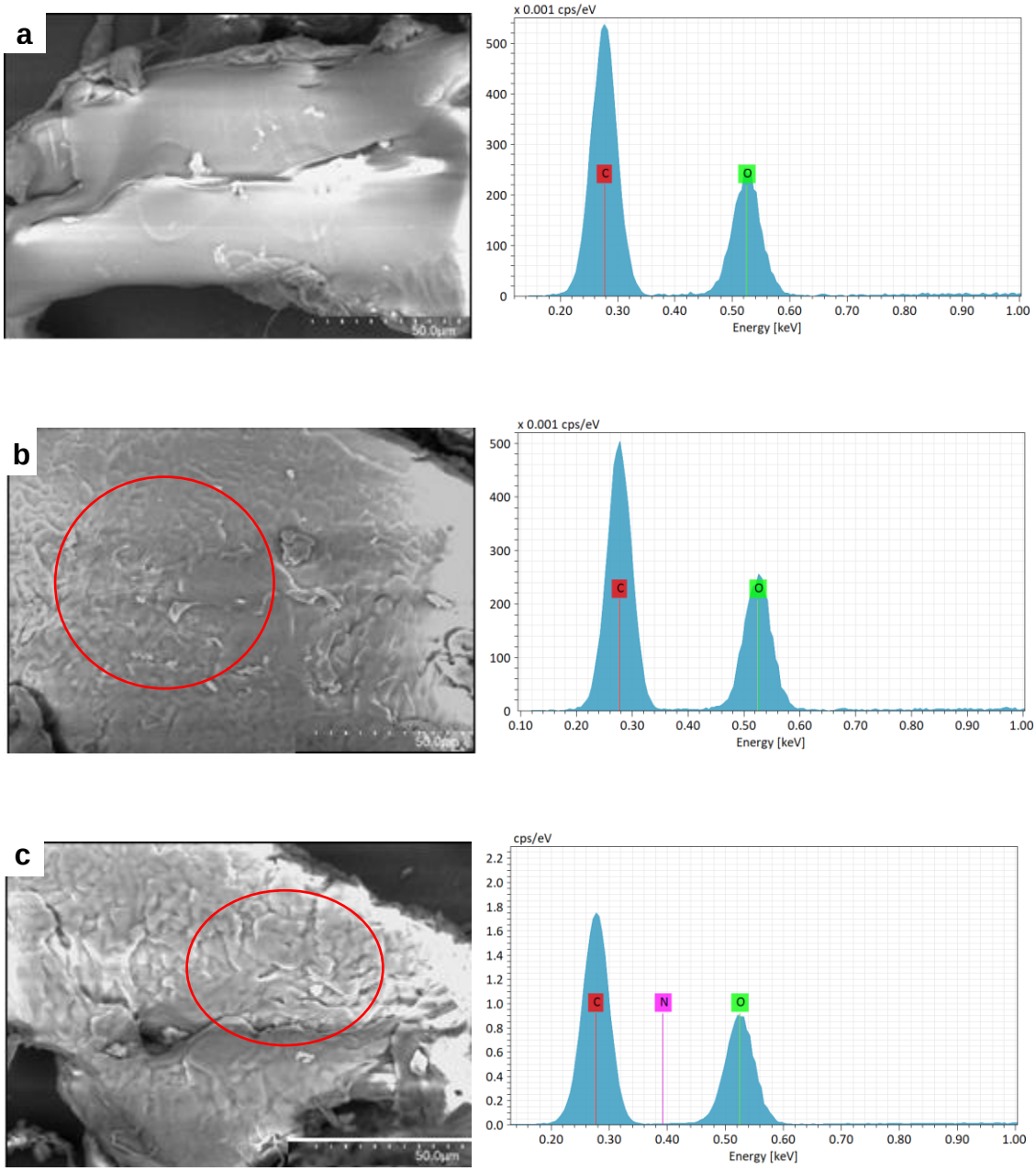

Fig. 4. SEM with EDX spectrum of (a) PLA + 0.5% cellulose; (b) PLA + 1% cellulose; (c) PLA + 2% cellulose at 800x magnification

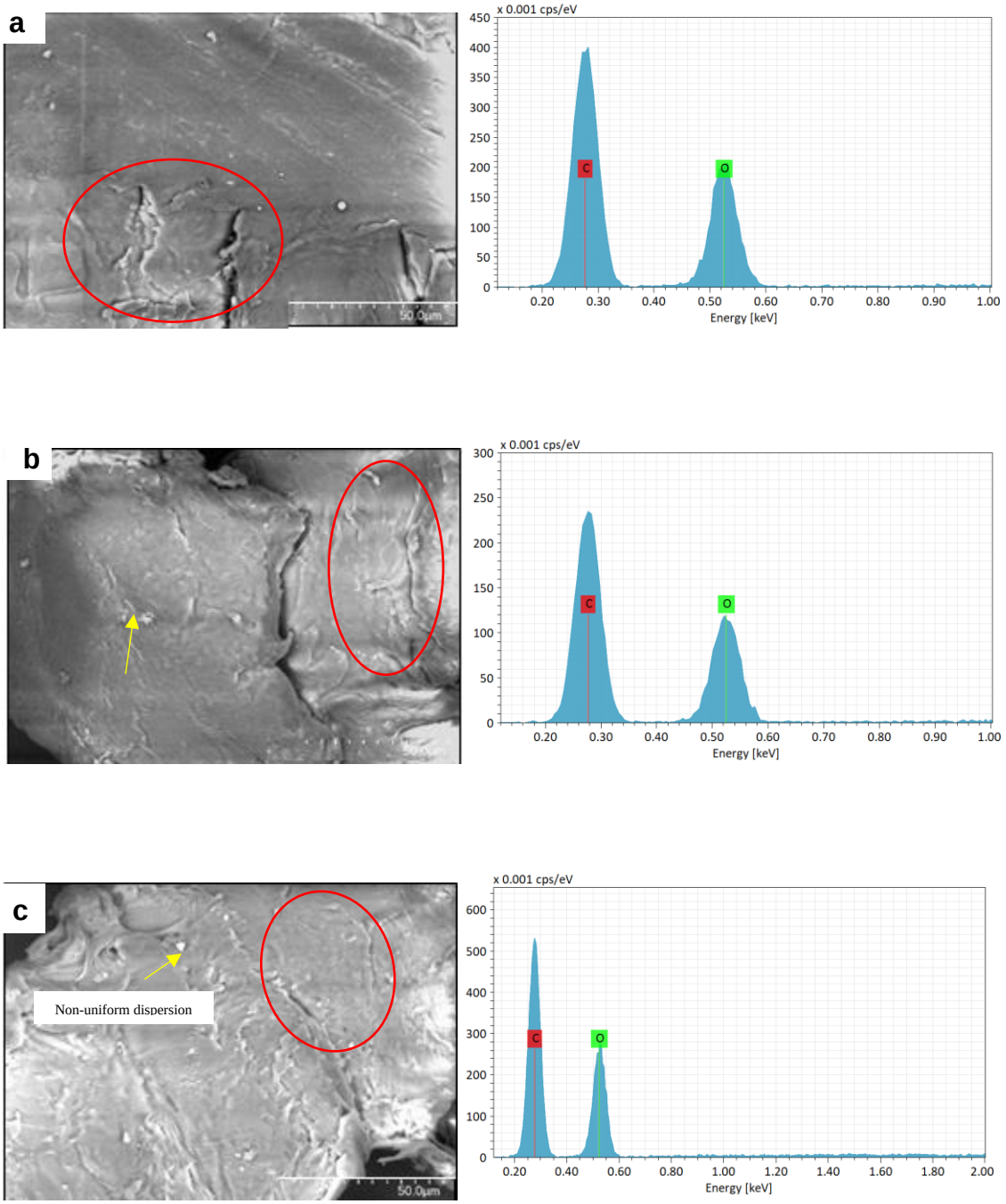

Fig. 5. SEM with EDX spectrum of (a) PLA + 2% cellulose + 0.5% AC; (b) PLA + 2% cellulose + 1% AC; (c) PLA + 2% cellulose + 2% AC at 800x magnification

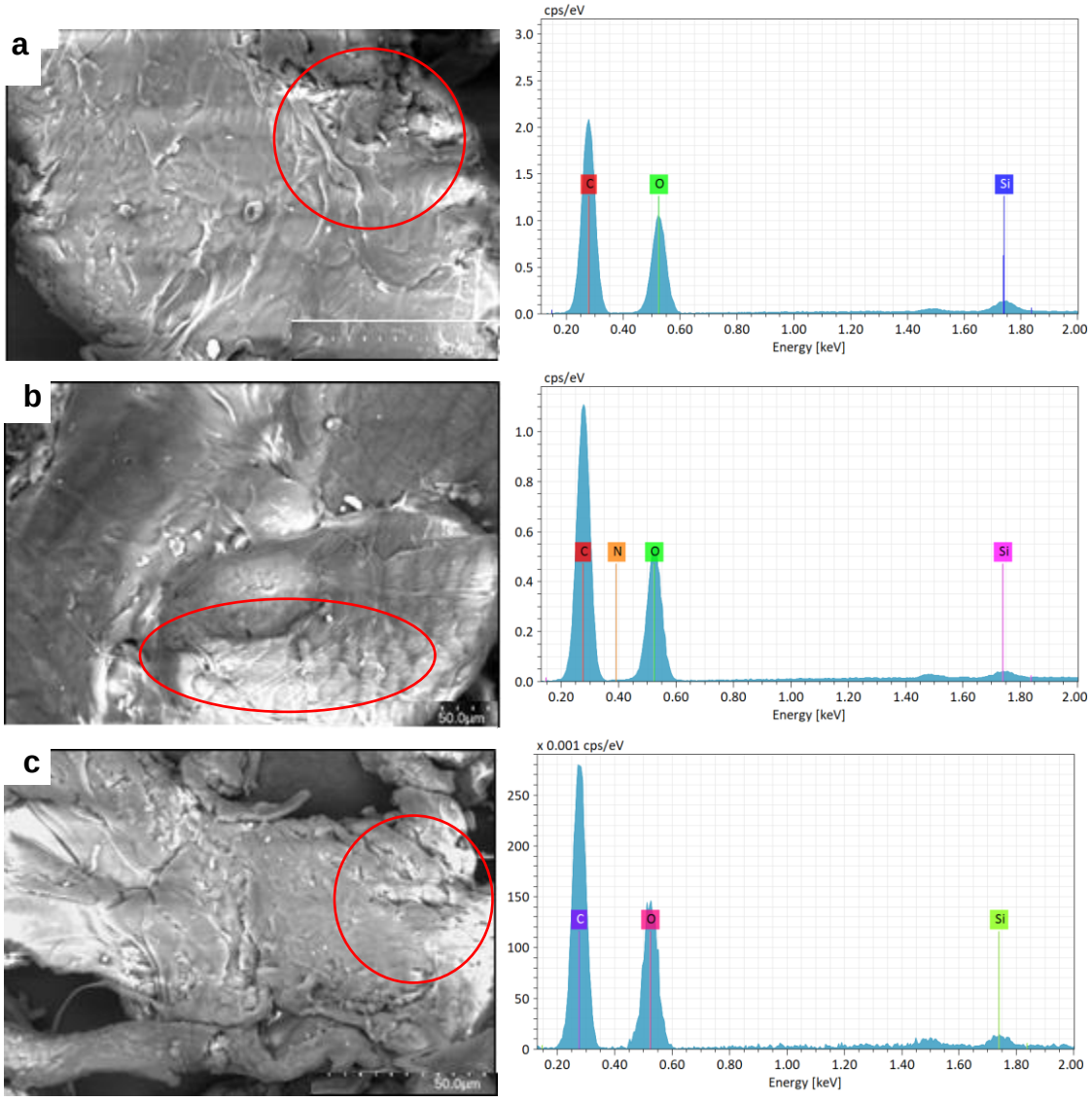

Fig. 6. SEM with EDX spectrum of (a) PLA + 1% cellulose + 1% AC + 1% MMT; (b) PLA + 2% cellulose + 1% AC + 1% MMT; (c) PLA + 2% cellulose + 2% AC +1% MMT at 800x magnification

Table 5. Elemental Composition Analysis Based on the EDX Spectra

Sample	Element (%)				Sum (%)
	C	N	O	Si	
Cellulose	53.44	1.71	44.85	-	100
Neat PLA	53.25	-	46.75	-	100
PLA + 0.5% cellulose	53.88	-	46.12	-	100
PLA + 1% cellulose	52.00	-	48.00	-	100
PLA + 2% cellulose	50.75	1.48	47.77	-	100
PLA + 2% cellulose + 0.5% AC	52.26	-	47.74	-	100
PLA + 2% cellulose + 1% AC	52.18	-	47.82	-	100
PLA + 2% cellulose + 2% AC	52.04	-	47.96	-	100
PLA + 1% cellulose + 1% AC + 1% MMT	52.69	-	46.27	1.04	100
PLA + 2% cellulose + 1% AC + 1% MMT	52.16	1.31	46.08	0.45	100
PLA + 2% cellulose + 2% AC + 1% MMT	52.76	-	46.68	0.56	100

Table 5 indicates the elements in the samples, which correlates with the EDX spectra shown in Figs. 2, 3, 4, 5, and 6. Carbon (C) and oxygen (O) were the most frequently detected elements in all samples, with C accounting for the highest percentage of elemental composition, followed by O. In addition, the table also shows the presence of nitrogen (N) in relatively low quantities in samples with high cellulose content. As an example, Fig. 2 exhibits 1.71% N, whereas Fig. 4 (c) and Fig. 6 (b) show 1.48% N and 1.31% N respectively.

This occurrence was attributed to the ability of cellulosic materials to permanently retain nitrogen compounds, albeit usually in a low percentage range due to the amino functions of the cellulose (Goto *et al.* 2021). Despite undergoing mild acidic washing which typically removes nitrogen compounds, certain nitrogen components remained resistant and tightly bound, leaving a small residue of nitrogen in the samples (Goto *et al.* 2021).

Additionally, the presence of MMT in samples depicted in Fig. 6 was associated with the presence of Silicon (Si) compounds. However, the amount was relatively low which accounted for 1.04%, 0.56%, and 0.45%. This can be attributed to the chemical structure of MMT which is a phyllosilicate mineral consisting of stacked layers where each layer is made up of two O-Si-O tetrahedral sheets sandwiching one O-Al(Mg)-O octahedral sheet (Zhou *et al.* 2019). The presence of Si due to MMT could also be seen in the FTIR spectra as explained previously for Fig. 1 (d) where Si-O stretching and bending were present.

BET analysis

Analysis of the nitrogen adsorption/desorption isotherms at 77 K, as in Figs. 7 (a), 8 (a), and 9(a), were conducted to estimate the specific surface areas of the prepared samples and their porosity, which correlate with their capabilities in removing dye molecules. Based on the displayed BET graphs, it was found that all of the adsorption/desorption curves were close to BET-type IV based on the International Union of Pure and Applied Chemistry (IUPAC) classification (Ambroz *et al.* 2018), which indicates the presence of both micro and mesopores on the surface of the samples with H2-type hysteresis loop.

The mesoporous structure has a relatively large surface area, including a high pore volume making the sample suitable for dye removal (Blachnio *et al.* 2021). The generated curves represent the characteristics of the pores and their sizes in which the SEM could not carry out the identification (Phothong *et al.* 2021). Based on the literature, the hysteresis loop for nitrogen at 77K occurs when the pores exceed 4 nm (Schlumberger and Thommes 2021). The appearance of the H2 hysteresis ring in Figs. 7(a), 8(a), and 9(a) signify the occurrence of pore blocking (Yuan *et al.* 2021).

The multi-point BET curves shown in Figs. 7 (b), 8(b), and 9(b) were used to determine the surface area of the mixtures, as tabulated in Table 6. The results show the addition of AC to PLA/cellulose mixtures increased the specific surface area of the samples from 0.297 m^2/g to 0.448 m^2/g. Further increment of specific surface area was obtained with the addition of 1% MMT, which reported 0.784 m^2/g.

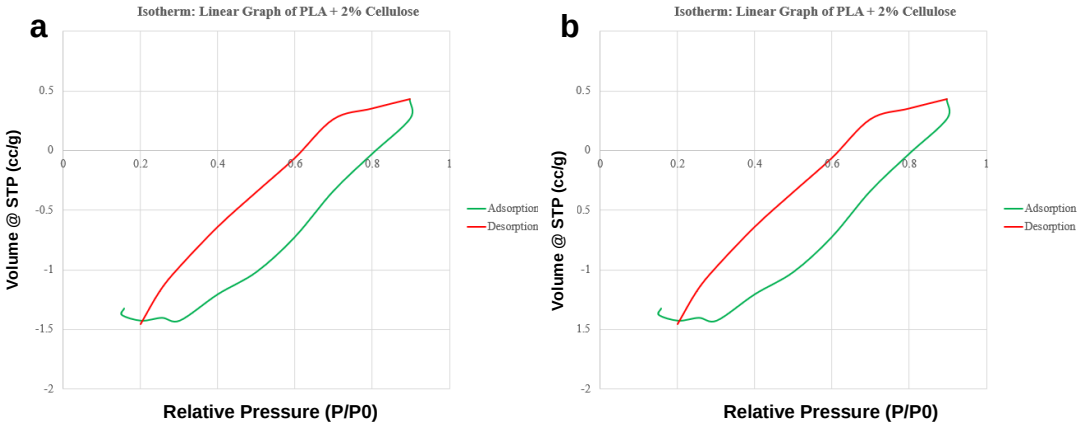

Fig. 7. Graph of (a) linear isotherm; (b) multi-point BET plot of PLA + 2% cellulose

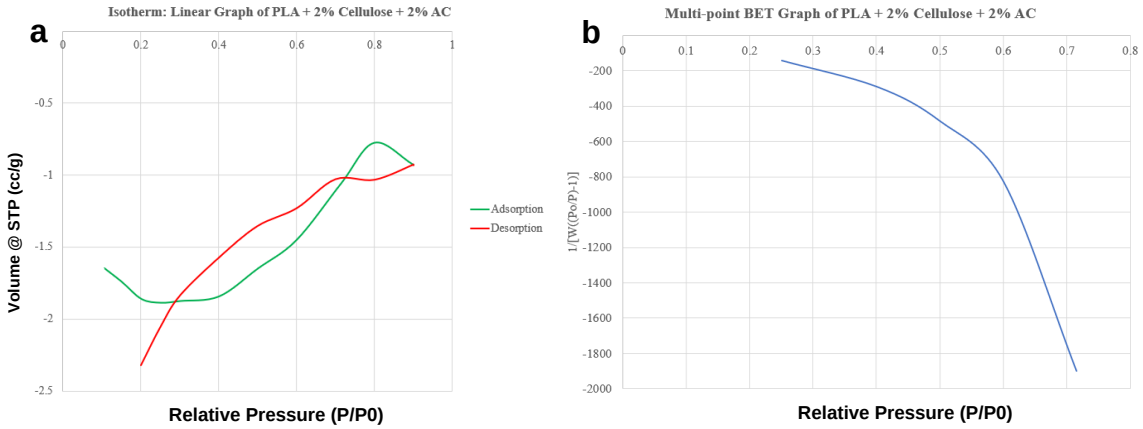

Fig. 8. Graph of (a) linear isotherm; (b) multi-point BET plot of PLA + 2% cellulose + 2% AC

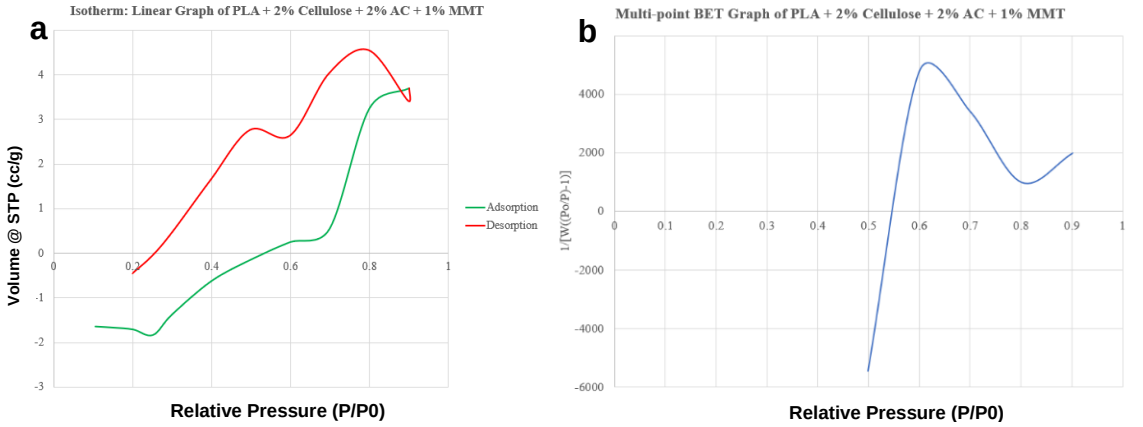

Fig. 9. Graph of (a) linear isotherm; (b) multi-point BET plot of PLA + 2% cellulose + 2% AC + 1% MMT

Table 6. Specific Surface Area (S_{BET})

Sample	Surface Area (m^2/g)
PLA + 2% cellulose	0.297
PLA + 2% cellulose + 2% AC	0.448
PLA + 2% cellulose + 2% AC + 1% MMT	0.784

TGA analysis

Thermogravimetric analysis was performed to determine the degradation temperature of the samples. As shown in Figs. 10 (a), (b), and (c)**,** different decomposition temperatures were observed in all samples. Each sample shows the evaporation of moisture from the cellulosic material at temperatures before 100 °C.

The finding aligned with the results of Sebeia *et al.* (2019). They reported the first degradation temperature was due to moisture evaporation bonded on the surface and the effect of hydrophilic material within the sample. Ruz-Cruz *et al.* (2022) supported the previous statement as the weight loss of their sample was noticed at the equivalent temperature, indicating the depolymerization of non-cellulosic materials due to the breakage of glycoside bonds. The appearance of the C-O-C peak in the FTIR spectra reflected the glycosidic bonds of non-cellulosic materials in the samples. The sample of PLA+0.5% cellulose has the highest value, and the thermal stability begins to decrease as the percentage of cellulose increases, as shown by the samples of PLA +1% cellulose and PLA+2% cellulose. This finding confirms the statement of Deng *et al*. (2020), who claimed that increasing the cellulose percentage in polymer composites significantly impacts TGA results. Several other factors that could influence the thermal stability of a sample include the functional groups, cross-linking, crystallinity, molecular weight, and branch degree (Tomic 2020).

Based on the calibration curve as illustrated in Fig. 10 (a), the weight loss of PLA + 1% cellulose and PLA + 2% cellulose were 15.8% and 14.6%, respectively, while PLA + 0.5% cellulose was 5.77%. At 350 °C, the PLA + 0.5% cellulose decomposition stage was much steeper, signifying that the sample decomposes quickly, with a total weight loss of 49.3%. In Fig. 10 (b), the decomposition of the PLA + cellulose + AC sample started at 250 °C. The PLA + 2% cellulose + 0.5% AC had a weight loss of 11.0%, while PLA + 2% cellulose + 1% AC recorded a weight loss of 21.7%. A greater weight loss was observed for sample PLA + 2% cellulose + 2% AC, with a weight loss of 96.1%. The weight loss observed in the sample PLA + 2% cellulose + 2% AC was attributed to the degradation of PLA and cellulose, while the AC remained stable. This can be explained by the carbonization process of AC which starts at a temperature as low as 400˚C. According to Salgado *et al.* (2018), the degradation of cellulose occurred throughout the entire heating process.

Additionally, the PLA polymer chain underwent thermal decomposition that contributed to a higher weight loss in the sample, similar to the finding of Silverajah *et al.* (2012). Besides, the increased percentage of AC to 2% aided in enhancing the degradation processes by providing a larger surface area for contact with degrading agents. Figure 10 (c) shows the decomposition of the PLA + cellulose + AC + MMT sample, which started around 300 °C, with the PLA + 2% cellulose + 2% AC + 1% MMT sample showing the steepest decomposition curve with a total weight loss of 71.4%. Incorporating a nanofiller, MMT clay, enhanced the microstructure uniformity of such samples, thereby increasing their thermal stability (Tomic 2020) and reducing the poor homogeneity and compatibility issues of most polymer composites (Nizamuddin *et al*. 2019).

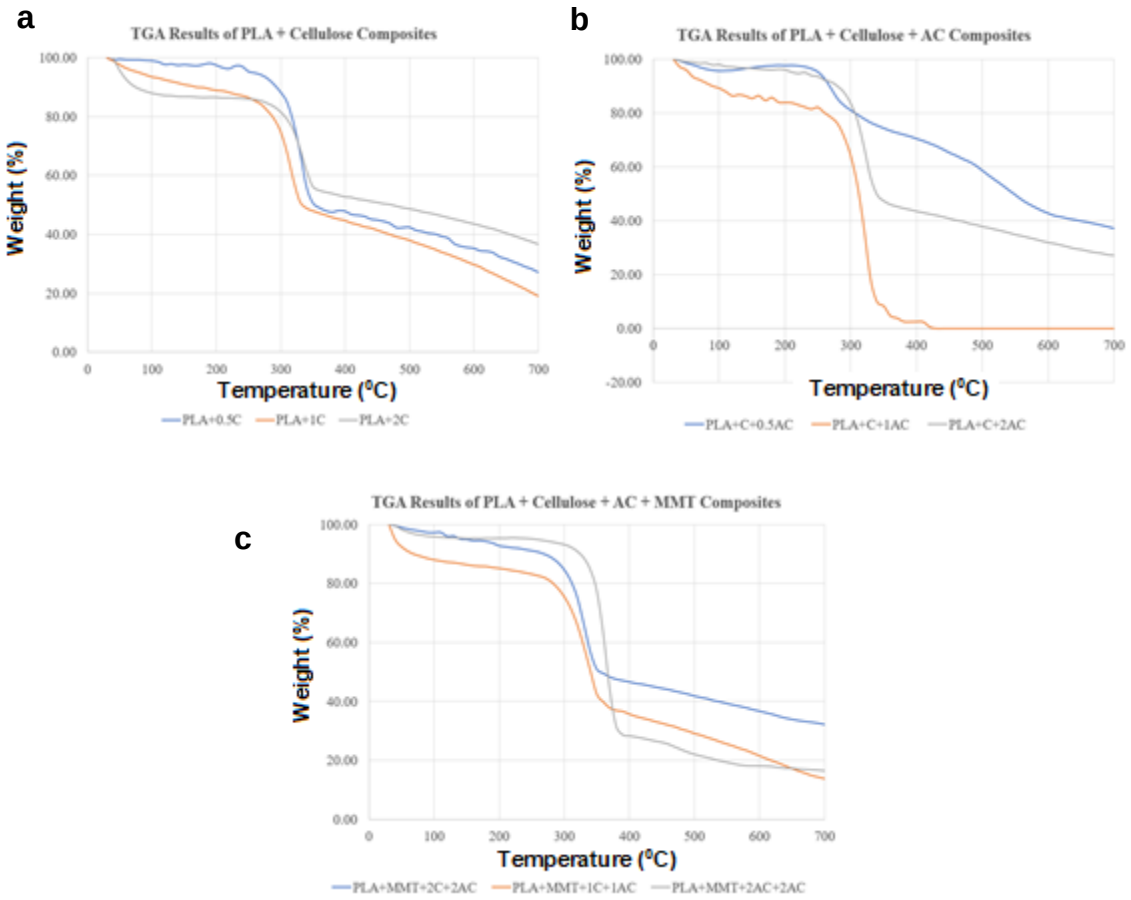

Fig. 10. Thermogravimetric analysis of (a) PLA + cellulose; (b) PLA + cellulose + AC; (c) PLA + cellulose + AC + MMT

Evaluation of the dye adsorption performance of the mixtures

UV-vis analysis was carried out by identifying the absorbance and concentration of the samples using the calibration curve. A calibration curve was plotted using 2, 6, 8, and 10 ppm of MB dye solution. The observation wavelength was set between 550 to 700 nm. Based on the findings, a wavelength of 664 nm was observed. Figure 11 displays the calibration graph of the MB dye solution, which was generated based on the absorbance value at the respective wavelength.

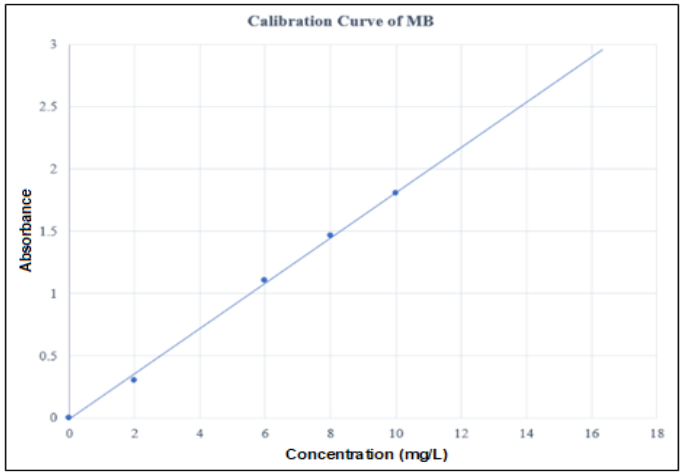

Fig. 11. Calibration curve of the MB dye solution

The calibration graph presented in Fig. 11 was used to determine the concentration of the samples. Following the determination of the concentrations, a graph of the effect of contact time on the efficiency of MB dye removal was plotted, as shown in Fig. 12. The analysis of the dye adsorption was done by varying the contact time between the samples with the dye solution. The adsorption performances of PLA + 2% cellulose, PLA + 2% cellulose + 2% AC and PLA + 2% cellulose + 2% AC + 1% MMT were investigated. The contact time for the adsorption of MB dye was set at 60 min with 10 min intervals for sample taking. The finding indicates that a high sorption rate was observed during the first 10 min for all samples, with sample PLA + 2% cellulose + 2% AC + 1% MMT showing the highest dye removal percentage. This was attributed to the abundance of available negatively charged active sites on the sample surface. The presence of 2% AC carbonaceous materials improves the morphological structure of the sample, leading to an increase in adsorption capacity (Goswami *et al.* 2022). According to Neethu and Choudhury (2018), MB is a cationic dye that carries positive charges. The removal of dye using microalgae mixtures was said to be more effective in alkaline pH solutions due to the greater adsorption of positively charged dyes that attracted the negatively charged surface (Lin *et al.* 2018; Mousavi *et al.* 2022). The presence of OH^- ions in the solution increases with rising pH levels, causing more protons to escape from the AC and react with hydroxyl ions, reinforcing the negatively charged surface of the adsorbent. Besides, the presence of carboxyl groups in the samples as detected in the FTIR results, also contributed to the formation of negative charges at higher pH levels, allowing cationic dyes to be electrostatically bound. Additionally, the presence of negatively charged functional groups on the surface of microalgae AC materials facilitates the ionic interaction between the MB and anionic moieties (Aragaw and Bogale 2021). Specifically, the ionic interaction occurs due to the electrostatic forces between positively charged MB molecules and negatively charged carboxylate ($-COO^-$) ions present on the surface of microalgae AC. As a result, the electrostatic force between the surface of the adsorbent and MB had been rendered more attractive, contributing to the effective adsorption of MB onto the microalgae AC (Pathania *et al.* 2017; Aragaw and Bogale 2021). However, after 10 min, the adsorption rate began to decrease due to the saturation of available sites on the surface of the adsorbent, resulting in equilibrium.

Sartape *et al*. (2017), Pathania *et al*. (2017), and Ambaye *et al*. (2020) stated that a decrease in adsorption efficiency indicates the formation of MB monolayer on the surface of the adsorbent, causing a lack of available sites for further MB uptake. Other factors such as initial dye concentration, pH, temperature, and contact time, provide a comprehensive understanding of the adsorption process and aid in optimizing the conditions for efficient dye removal (Aragaw and Bogale 2021; Banerjee and Chattopadhyaya 2017).

Based on the comparison in Fig. 12, the sample of PLA + 2% cellulose + 2% AC + 1% MMT shows the highest reduction of MB dye which accounted for 86.8% with a final dye concentration of 6.6 mg/L after removal. This corresponds to an approximately 43.4 mg g^{-1} of dye adsorption capacity after 60 minutes of contact time. The findings indicate that the sample of PLA + 2% cellulose + 2% AC + 1% MMT outperformed the PLA/cellulose and PLA/cellulose/AC samples in terms of adsorption capacity. Comparative studies as summarised in Table 7 were conducted to further evaluate the performance of the developed sample (PLA + 2% cellulose + 2% AC + 1% MMT) in comparison to other materials.

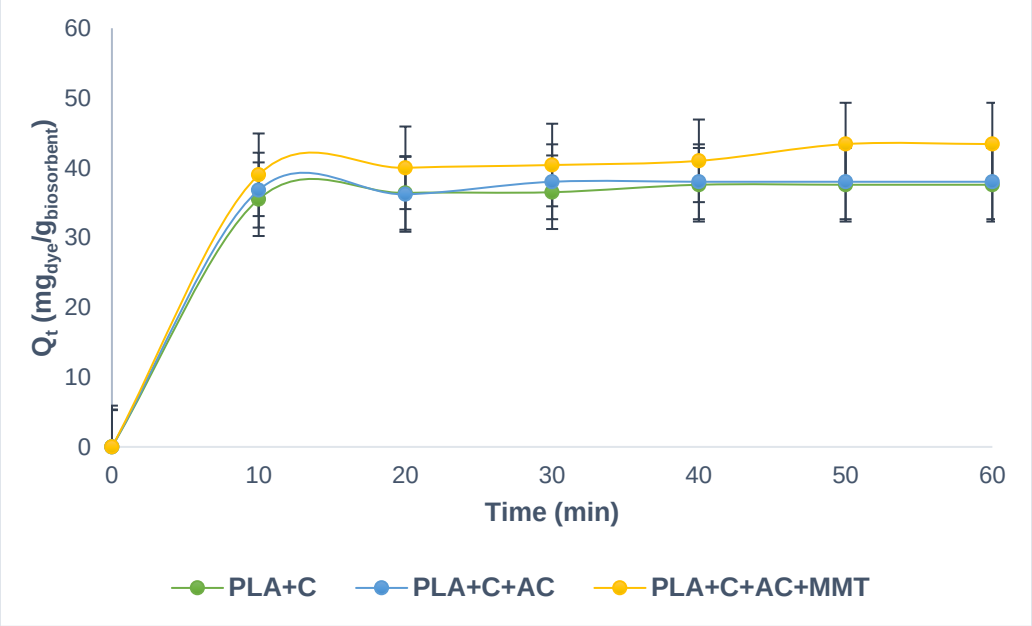

Fig. 12. Effect of the samples contact time on MB dye adsorption at ambient temperature 30 °C

Table 7. Comparative Analysis of Methylene Blue Dye Adsorption Capacities in Previous Studies Using Various Adsorbents

Adsorbent	Experimental conditions	Adsorption capacity (Q_t)	References
Nano-activated carbon (NAC) from industrial mine coal	*m*:1 g/L C_O: 50mg/L *t*: N/A; pH:7	Q_t: 28.1 mg/g	Shokry *et al*. (2019)
Commercial activated carbon and apricot stones	*m*:10 g/L C_O: 10mg/L *t*: 60-180 min pH: 4.85	Commercial activated carbon Q_t: 199.6 mg/g Activated carbon prepared from apricot stones Q_t: 36.7 mg/g	Djilani *et al*. (2015)
Neem sawdust	*m*:5 g/L C_O: 6-12 mg/L *t*: 30 min; pH: 7.2	2.12 mg/g	Khattri and Singh (2000)
Spent substrate of *Pleurotus eryngii* (mushroom)	*m*: N/A C_O: 100 mg/L *t*: 240 min; pH: 6	22.4 mg/g	Wu *et al*. (2019)
Cross-linked chitosan/sepiolite (hybrids)	*m*:2 g/L C_O: 25 - 400 mg/L *t*: 1800 min pH: 3 - 11	41.0 mg/g	Marrakchi *et al*. (2016)
Fly ash biomass (Biomass fly ash geopolymer monoliths) (hybrids)	*m*: 2 g/L C_O: 1-50 mg/L *t*: 1800 min pH: N/A	15.4 mg/g	Novais *et al*. (2018)
PLA + 2% cellulose + 2% AC + 1% MMT (This study)	*m*: 1 g/L C_O: 50 mg/L *t*: 60 min pH: N/A	43.4 mg/g	-

m: Adsorbent dose; C_o: Initial dye concentration; *t*: time; Q_t: adsorption capacity

The findings provided evidence that the developed sample (PLA + 2% cellulose + 2% AC + 1% MMT) could be considered a promising adsorbent for the removal of MB dye. Based on the comparison, the amount of MB removed by the sample (PLA + 2% cellulose + 2% AC + 1% MMT) is comparable to that removed by previous studies, with the MB adsorption capacity of the sample being slightly higher with a low dosage of adsorbent (1 g/L) than that of the other studies listed in Table 7. However, when compared to the effectiveness of commercial activated carbon (CAC) in removing MB dye from an aqueous solution, the performance of the developed sample was still low. Although CAC is exceptionally efficient at removing MB dye, its high cost is a significant barrier for large-scale applications, particularly in industries. It has been demonstrated that a high percentage of cellulose and AC significantly impact the uptake of dye molecules, similar to the findings reported by other authors (Blachnio *et al.* 2021). The porous structure and large surface area of activated carbon provide the sample with numerous vacant sites for the adsorption of dye molecules to take place. Besides, excellent homogeneity in MMT clay dispersion with fine particle size on the sample's surface has improved the potential of dye removal due to its high surface area. Apart from that, MMT also can remove the presence of hydrophilic cationic pollutants (Kryuchkova *et al.* 2021). According to several studies, MMT clay has a high porosity and excellent cation exchange capacity, making it an adsorbent material (Oktay *et al.* 2016; Klunk *et al.* 2019). The described sample

characteristic was correlated with the sample's BET analysis, which recorded the highest specific surface area.

In contrast, the dye solution samples taken after adsorption by sample PLA + C show the lowest absorbance value of 2 (Fig. 12). It means that the amount of light absorbed by the dye solution from the adsorption process was lower than in other samples. As a result, the final adsorption capacity was approximately 37.6 mg/g after 60 minutes of contact time.

CONCLUSIONS

1. The incorporation of *Arthrospira platensis (Spirulina)* microalgae cellulose, Dabai activated carbon, and montmorillonite (MMT) into a poly(lactic acid) (PLA) matrix without significant agglomeration suggests their compatibility and potential for efficient methylene blue (MB) dye removal from an aqueous solution.
2. The presence of distinct functional groups within the biosorbent, such as C=O variations in microalgae cellulose and the presence of a Si-O peak in MMT, indicates favorable binding sites and strong adhesion interaction.
3. The scanning electron microscope (SEM) analysis showed the coarse surface morphology of the biosorbent, revealing both mesopores and micropores structures observed in the Brunauer-Emmett-Teller (BET) analysis. Incorporating MMT and activated carbon (AC) provided additional surface area and a porous structure to the biosorbent which enhances its dye adsorption capacity by providing ample trapping sites and an increased surface area.
4. The addition of 2% microalgal cellulose, 2% Dabai AC, 1% MMT into PLA matrix resulted in the highest adsorption capacity with 86.8% reduction in MB dye concentration, reducing it to 6.6 mg/L after 60 mins of contact time. The adsorption capacity of this mixture was approximately 43.3 mg/g, outperforming the PLA/cellulose and PLA/cellulose/AC samples. Comparative studies further support the promising performance of the developed mixture as a biosorbent for MB dye removal.
5. The finding of this study implies that the combination of algae cellulose, Dabai AC, and MMT to the PLA matrix synergistically contributes to the effective removal of MB dye molecules by providing a suitable matrix, favorable binding sites, increased surface area and diverse adsorption mechanisms.

ACKNOWLEDGMENTS

This research work was funded by Institutional Fund Projects under grant no (IFPIP-301-130-1443). The authors gratefully acknowledge technical and financial support provided by the ministry of Education and King Abdulaziz University, DSR, Jeddah, Saudi Arabia.

REFERENCES CITED

Aka, E., Nongbe, M., Ekou, T., Ekou, L., Coeffard, V., and Felpin, F. (2019). "A fully bio-sourced adsorbent of heavy metals in water fabricated by immobilization of quinine on cellulose paper," *Journal of Environmental Sciences* 84(1), 174-183. DOI: 10.1016/j.jes.2019.05.006

Ambaye, T., Vaccari, M., Hullebusch, E., Amrane, A., and Rtimi, S. (2020). "Mechanisms and adsorption capacities of biochar for the removal of organic and inorganic pollutants from industrial wastewater," *International Journal of Environmental Science and Technology* 18(1), 3273-3294. DOI: 10.1007/s13762-020-03060-w

Ambroz, F., Macdonald, T. J., Martis, V., and Parkin, I. (2018). "Evaluation of the BET theory for the characterization of meso and microporous MOFs," *Small Methods* 2(11), 1-18. DOI: 10.1002/smtd.201800173

Aragaw, T. A., and Bogale, F. M. (2021). "Biomass-based adsorbents for removal of dyes from wastewater: A review," *Frontiers in Environmental Science* 9, article 764958. DOI: 10.3389/fenvs.2021.764958

Arjmandi, R., Hassan, A., Haafiz, M. M., and Zakaria, Z. (2016). "Effect of micro and nano-cellulose on tensile and morphological properties of montmorillonite nanoclay reinforced polylactic acid nanocomposites," *Nanoclay Reinforced Polymer Composites*. 103-125. DOI: 10.1007/978-981-10-0950-1_5

ASTM D6556-14 (2014). "Standard test method for carbon black - Total and external surface area by nitrogen adsorption," ASTM International, West Conshohocken, PA, USA.

ASTM E1252-98 (2021). "Standard practice for general techniques for obtaining infrared spectra for qualitative analysis," ASTM International, West Conshohocken, PA

ASTM E1131-20 (2020). "Standard test method for compositional analysis by thermogravimetry," ASTM International, West Conshohocken, PA.

ASTM E168-16 (2016). "Standard practices for general techniques of infrared quantitative analysis," ASTM International, West Conshohocken, PA.

ASTM E169-16 (2016). "Standard practices for general techniques of ultraviolet-visible quantitative analysis," ASTM International, West Conshohocken, PA, USA.

ASTM E2015-04 (2014). "Standard guide for the preparation of plastics and polymeric specimens for microstructural examination," ASTM International, West Conshohocken, PA.

Alshahrani, A., Alorabi, A., Hassan, M., Amna, T., and Azizi, M. (2022). "Chitosan-functionalized hydroxyapatite-cerium oxide heterostructure: An efficient adsorbent for dyes removal and antimicrobial agent," *Nanomaterials* 12(15), 1-18. DOI: 10.3390/nano12152713

Banerjee, S., and Chattopadhyaya, M. C. (2017). "Adsorption characteristics for the removal of a toxic dye, tartrazine from aqueous solutions by a low cost agricultural by-product," *Arabian Journal of Chemistry* 10(2), S1629-S1638. DOI: 10.1016/j.arabjc.2013.06.005

Berber-Villamar, N., Netzahuatl-Munoz, A., Morales-Barrera, L., Chavez-Camarillo, G., Florez-Ortiz, C., and Cristiani-Urbina, E. (2018). "Corncob as an effective, eco-friendly, and economic biosorbent for removing the azo dye direct yellow 27 from aqueous solutions," *PLoS ONE* 13(4) 1-18. DOI: 10.1371/journal.pone.0196428

Biswas, S., and Pal, A. (2021). "Application of biopolymers as a new age sustainable material for surfactant adsorption: A brief review," *Carbohydrate Polymer Technologies and Applications* 2(1), 1-18. DOI: 10.1016/j.carpta.2021.100145

Blachnio, M., Derylo-Marczewska, A., Winter, S., and Zienkiewicz-Strzalka, M. (2021). "Mesoporous carbons of well-organized structure in the removal of dyes from aqueous solutions," *Molecules* 26(8) 1-15. DOI: 10.3390/molecules26082159

Chieng, B., Ibrahim, N., Yunus, W., and Hussein, M. (2013). "Effects of graphene nanoplatelets of poly (lactic acid)/ poly (ethylene glycol) polymer nanocomposites," *Polymers* 6(1), 93-104. DOI: 10.3390/polym6010093

Choksi, N., and Desai, H. (2017). "Synthesis of biodegradable polylactic acid polymer by using lactic acid monomer," *International Journal of Applied Chemistry* 13(2), 377-384.

Deng, J., Xu, L., Liu, J., Peng, J., Han, Z., Shen, Z., and Guo, S. (2020). "Efficient method of recycling carbon fiber from the waste of carbon fiber reinforced polymer composites," *Polymer Degradation and Stability* 182(1), 1-15. DOI: 10.1016/j.polymdegradstab.2020.109419

Djilani, C., Zaghdoudi, R., Djazi, F., Bouchekima, B., Lallam, A., Modarressi, A., and Rogalski, M. (2015). "Adsorption of dyes on activated carbon prepared from apricot stones and commercial activated carbon," *Journal of Taiwan Institute of Chemical Engineering* 53, 112-121. DOI:10.1016/j.jtice.2015.02.025

Goswami, L., Kushwaha, A., Kafle, S., and Kim, B. S. (2022). "Surface modification of biochar for dye removal from wastewater," *Catalysts* 12(8), 1-17. DOI: 10.3390/catal12080817

Goto, T., Zaccaron, S., Bacher, M., Hettegger, H., Potthast, A., and Rosenau, T. (2021). "On nitrogen fixation and 'residual nitrogen content' in cellulosic pulps," *Carbohydrate Polymers* 253, article 117235.

Harja, M., Buema, G., and Bucur, D. (2022). "Recent advances in removal of Congo Red dye by adsorption using an industrial waste," *Scientific Reports* 12(1), 6087, 1-18. DOI: 10.1038/s41598-022-10093-3

Hong, T., Yin, J. Y., Nie, S. P., and Xie, M. Y. (2021). "Applications of infrared spectroscopy in polysaccharide structural analysis: Progress, challenge and perspective," *Food Chemistry: X* 12(1), 1-16. DOI: 10.1016/j.fochx.2021.100168

Hospodarova, V., Singovska, E., and Stevulova, N. (2018). "Characterization of cellulosic fibers by FTIR spectroscopy for their further implementation to building materials," *American Journal of Analytical Chemistry* 9(6), 303-310. DOI: 10.4236/ajac.2018.96023

James, A., Rahman, M.R., Huda, D., Aqlan, F., Matin, M., Bakri, M. K. B., and Rahman, M. (2022). "Synthesis and characterization of novel nano-carbon mixture from Dabai (*Canarium odontophyllum*) nutshell," *BioResources* 17(3), 4452-4469. DOI: 10.15376/biores.17.3.4452-4469

James, A., Rahman, M. R., Huda, D., Rahman, M. M., Uddin, J., Bakri, M. K., and Chanda, A. (2023). "Optimization of novel nanocomposite powder for simultaneous removal of heavy metals from palm oil mill effluent (POME) by response surface methodology (RSM)," *Environment Development and Sustainability*. DOI: 10.1007/s10668-022-02849-8

Kannam, S., Oehme, D., Doblin, M., Gidley, M., Bacic, A., and Downton, M. (2017). "Hydrogen bonds and twist in cellulose microfibrils," *Carbohydrate Polymers* 175(1), 433-439. DOI: 10.1016/j.carbpol.2017.07.083

Khattri, S. D., and Singh, M. K. (2000). "Colour removal from synthetic dye wastewater using a biosorbent," *Water, Air, and Soil Pollution* 120, 283-294. DOI: 10.1023/A:1005207803041

Khui, P., Rahman, M., Ahmed, A., Kuok, K., Bakri, M. K. B., Tazeddinova, D., and Baibatyrov, T. (2021). "Morphological and thermal properties of composites prepared with poly (lactic acid), poly (ethylene-alt-maleic anhydride) and biochar from microwave-pyrolyzed jatropha seeds," *BioResources* 16(2), 3171-3184. DOI: 10.15376/biores.16.2.3171-3185

Klunk, M. A., Antonio, Shah, Z., Wander, P., and Roberto, P. (2019). "Use of montmorillonite clay for adsorption malachite green dye," *Periodico Tche Quimica* 16(31), 279-286.

Kryuchkova, M., Batasheva, S., Akhatova, F., Babaev, V., Buzyurova, D., Vikulina, A., and Rozhina, E. (2021). "Pharmaceuticals removal by adsorption with montmorillonite nanoclay," *International Journal of Molecular Sciences* 22(18), 1-15. DOI: 10.3390/ijms22189670

Lin, Y., Ho, S., Zhou, Y., and Ren, N. (2018). "Highly efficient adsorption of dyes by biochar derived from pigments-extracted macroalgae pyrolyzed at different temperature," *Bioresource Technology* 259(1), 104-110. DOI: 10.1016/j.biortech.2018.02.094

Mallamace, F., Carsaro, C., Mallamace, D., Vasi, S., Vasi, C., and Dugo, G. (2014). "The role of water in protein's behavior: The two dynamical crossovers studied by NMR and FTIR techniques," *Computational and Structural Biotechnology Journal* 13. DOI: 10.1016/j.csbj.2014.11.007

Marrakchi, F., Khanday, W. A., Asif, M., and Hameed, B. H. (2016). "Cross-linked chitosan/sepiolite composite for the adsorption of methylene blue and reactive orange 16". *International Journal of Biological Macromolecules* 93, 1231-1239. DOI: 10.1016/j.ijbiomac.2016.09.069

Moghazy, R., and Abdo, S. (2018). "The efficacy of microalgal biomass collected from high rate algae pond for dyes biosorption and biofuel production," *Research Journal of Chemistry and Environment* 22(11), 54-60.

Moghazy, R., Labena, A., Husien, S., Mansor, E., and Abdelhamid, A. (2020). "Neoteric approach for efficient eco-friendly dye removal and recovery using algal-polymer biosorbent sheets: Characterization, factorial design, equilibrium and kinetics," *International Journal of Biological Macromolecules* 157(1), 494-509. DOI: 10.1016/j.ijbiomac.2020.04.165

Moradihamedani, P. (2021). "Recent advances in dye removal from wastewater by membrane technology: A review," *Polymer Bulletin* 79(1), 2603-2631. DOI: 10.1007/s00289-021-03603-2

Mousavi, S., Mahmoudi, A., Amiri, S., Darvishi, P., and Noori, E. (2022). "Methylene blue removal using grape leaves waste: Optimization and modeling," *Applied Water Science* 12(1), 1-11. DOI: 10.1007/s13201-022-01648-w

Neethu, N., and Choudhury, T. (2018). "Treatment of methylene blue and methyl orange dyes in wastewater by grafted titania pillared clay membrane". *Recent Patents on Nanotechnology* 12(3), 200-207. DOI: 10.2174/1872210512666181029155352

Nidheesh, P., Zhou, M., and Oturan, M. (2018). "An overview on the removal of synthetic dyes from water by electrochemical advanced oxidation processes," *Chemosphere* 197(1), 210-227. DOI: 10.1016/j.chemosphere.2017.12.195

Nizamuddin, S., Jadhav, A., Qureshi, S., Baloch, H., Siddique, M., Mubarak, N., and

Ahamed, M. (2019). "Synthesis and characterization of polylactide/rice husk hydrochar composite," *Scientific Reports* 9(1), 1-10. DOI: 10.1038/s41598-019-41960-1

Novais, R. M., Ascensao, G., Tobaldi, D. M., Seabra, M. P., and Labrincha, J. A. (2018). "Biomass fly ash geopolymer monoliths for effective methylene blue removal from wastewaters". *Journal of Cleaner Production* 171, 783-794. DOI: 10.1016/j.jclepro.2017.10.078

Oktay, B., Coruh, S., and Elevli, S. (2016). "Malachite green dye removal using montmorillonite clay: Full factorial design analysis," *International Journal of Advances in Science Engineering and Technology* 4(3), 13-17.

Paska, O., Pacurariu, C., and Muntean, S. (2014). "Kinetic and thermodynamic studies on methylene blue biosorption using corn-husk," *RSC Advances* 4(107), 62621-62630. DOI: 10.1039/c4ra10504d

Patel, H. A., Somani, R. S., Bajaj, H. C., and Jasra, R. V. (2006). "Nanoclays for polymer nanocomposites, paints, inks, greases and cosmetics formulations, drug delivery vehicle and waste water treatment," *Bulletin of Materials Science* 29(2), 133-145. DOI: 10.1007/BF02704606

Pathania, D., Sharma, S., and Singh, P. (2017). "Removal of methylene blue by adsorption onto activated carbon developed from *Ficus carica* bast," *Arabian Journal of Chemistry* 10(1), S1445-S1451. DOI: 10.1016/j.arabjc.2013.04.021

Phothong, K., Tangsathitkulchai, C., and Lawtae, P. (2021). "The analysis of pore development and formation of surface functional groups in bamboo-based activated carbon during CO_2 activation," *Molecules* 26(18), 1-15. DOI: 10.3390/molecules26185641

Qi, X., Tong, X., Pan, W., Zeng, Q., You, S., and Shen, J. (2021). "Recent advances in polysaccharide-based adsorbents for wastewater treatment," *Journal of Cleaner Production* 315(1), article 128221. DOI: 10.1016/j.jclepro.2021.128221

Ramesh, P., Prasad, B., and Narayana, K. (2019). "Effect of MMT clay on mechanical, thermal and barrier properties of treated aloevera fiber/PLA-hybrid biocomposites," *Silicon* 12(1), 1751-1760. DOI: 10.1007/s12633-019-00275-6

Rocca-Smith, J., Lagorce-Tachon, A., Laconelli, C., Bellat, J., Marcuzzo, E., Sensidoni, A., and Karbowiak, T. (2017). "How high pressure CO_2 impacts PLA film properties," *eXPRESS Polymer Letters* 11(4), 320-333. DOI: 0.3144/expresspolymlett.2017.31

Royanudin, M., Utomo, Y., and Wonorahardjo, S. (2021). "The application of silica-cellulose material as heavy metal adsorbent on laboratory wastewater," *AIP Conference Proceedings* 2353(1), 1-7. DOI: 10.1063/5.0052808

Ruz-Cruz, M., Herrera-Franco, P., Flores-Johnson, E., Moreno-Chulim, M., Galera-Manzano, L., and Valadez-Gonzalez, A. (2022). "Thermal and mechanical properties of PLA-based multiscale cellulosic biocomposites," *Journal of Materials Research and Technology* 18(1), 485-495. DOI: 10.1016/j.jmrt.2022.02.072

Salgado, M. F., Abioye, A. M., Junoh, M. M., Santos, J. A. P., and Ani, F. N. (2018). "Preparation of activated carbon from babassu endocarpunder microwave radiation by physical activation," *IOP Conference Series Earth and Environmental Science* 105(1), article 012116. DOI: 10.1088/1755-1315/105/1/012116

Samia, B. H., Bey, B. H. M., Scheherazade, K., and El- Amine, A. A. S. M. (2016). "Physicochemical analysis of cellulose from microalgae *Nannochloropsis gaditana*," *African Journal of Biotechnology* 15(24), 1201-1207. DOI: 10.5897/AJB2016.15321

Samsami, S., Mohamadizaniani, M., Sarrafzadeh, M.-H., Rene, E. R., and Firoozbahr, M. (2020). "Recent advances in the treatment of dye-containing wastewater from textile industries: Overview and perspectives," *Process Safety and Environmental Protection* 143(1), 138-163. DOI: 10.1016/j.psep.2020.05.034

Sartape, A., Mandhare, A., Jadhav, V., Raut, P., Anuse, M., and Kolekar, S. (2017). "Removal of malachite green dye from aqueous solution with adsorption technique using Limonia acidissima (wood apple) shell as low cost adsorbent," *Arabian Journal of Chemistry* 10(2), S3229-S3238. DOI: 10.1016/j.arabjc.2013.12.019

Schlumberger, C., and Thommes, M. (2021). "Characterization of hierarchically ordered porous materials by physisorption and mercury porosimetry," *Advanced Materials Interfaces* 8(4), 1-25. DOI: 10.1002/admi.202002181

Sebeia, N., Jabli, M., Ghith, A., Elghoul, Y., and Alminderej, F. (2019). "Production of cellulose from Aegagropila Linnaei macro-algae: Chemical modification, characterization and application for the bio-sorption of cationic and anionic dyes from water," *International Journal of Biological Macromolecules* 135(1), 152-162. DOI: 10.1016/j.ijbiomac.2019.05.128

Shokry, H., Elkady, M., and Hamad, H. (2019). "Nano activated carbon from industrial mine coal as adsorbents for removal or dye from simulated textile wastewater: Operational parameters and mechanism study," *Journal of Materials Research and Technology* 8(5), 4477-4488. DOI: 10.1016/j.jmrt.2019.07.061

Siddiqui, S. I., Fatima, B., Tara, N., Rathi, G., and Chaudhry, S. A. (2019). "Recent advances in remediation of synthetic dyes from wastewaters using sustainable and low-cost adsorbents," in: *The Impact and Prospects of Green Chemistry for Textile Technology* 2019, 471-507. DOI: 10.1016/B978-0-08-102491-1.00015-0

Silverajah, V. S. G., Ibrahim, N. A., Yunus, W. M. Z. W., Hassan, H. A., Chieng, B. W. (2012). "A comparative study on the mechanical, thermal and morphological characterization of poly(lactic acid)/ epoxidized palm oil blend," *International Journal of Molecular Sciences* 13(5), 5878-5898. DOI: 10.3390/ijms13055878

Singh, N. B., Nagpal, G., Agrawal, S., and Rachna. (2018). "Water purification by using adsorbents: A review," *Environmental Technology & Innovation* 11, 187-240. DOI: 10.1016/j.eti.2018.05.006

Slama, H., Bouket, A., Pourhassan, Z., Alenezi, F., Silini, A., Cherif-Silini, H., and Belbahri, L. (2021). "Diversity of synthetic dyes from textile industries, discharge impacts and treatment methods," *Applied Sciences* 11(14), 1-21. DOI: 10.3390/app11146255

Sousa, S., Costa, A., Silva, A., and Simoes, R. (2019). "Poly (lactic acid)/ cellulose films produced from composite spheres prepared by emulsion-solvent evaporation method," *Polymers* 11(1), 1-19. DOI: 10.3390/polym11010066

Sultana, M., Rownok, M., Sabrin, M., Rahaman, M., and Alam, S. (2022). "A review on experimental chemically modified activated carbon to enhance dye and heavy metals adsorption," *Cleaner Engineering and Technology* 6(10). 1-14. DOI: 10.1016/j.clet.2021.100382

Tomic, N. (2020). "Thermal studies of compatibilized polymer blends," in: *Compatibilization of Polymer Blends: Micro and Nano Scale Phase Morphologies, Interphase Characterization and Properties*, A.R. Ajitha and S. Thomas (eds.), Elsevier, Amsterdam, Ch.17, pp. 489-510. DOI: 10.1016/B978-0-12-816006-0.00017-7

Wu, J., Xia, A., Chen, C., Feng, L., Xiaohui, S., and Wang, X. (2019). "Adsorption thermodynamics and dynamics of three typical dyes onto bio-adsorbent spent substrate of *Pleurotus eryngii*," *International Journal of Environmental Research and Public Health* 16(5), 679. DOI: 10.3390/ijerph16050679

Yuan, Y., Cai, F., and Yang, L. (2021). "Pore structure characteristics and fractal structure evaluation of medium and high-rank coal," *Energy Exploration & Exploitation* 40(1), 1-10. DOI: 10.1177/01445987211034315

Zhou, C., Tong, D., and Yu, W. (2019). "Smectite nanomaterials: Preparation, properties, and functional applications," in: *Nanomaterials from Clay Minerals*, Elsevier, pp. 335-364.

Article submitted: April 20, 2023; Peer review completed: May 13, 20203; Revised version received: July 3, 2023; Accepted: July 7, 2023; Published: July 18, 2023.
DOI: 10.15376/biores.18.3.5967-5992